Indian Journal of Pure & Applied Physics
Vol. 55, July 2017, pp. 512-517

Catalyst-free growth and luminescence response of single-crystalline ZnO nanorods

Sayan Bayan, Lalmohan Pegu & Dambarudhar Mohanta*

Nanoscience and Soft Matter Laboratory, Department of Physics, Tezpur University, Tezpur, Assam 784 028, India

Received 9 March 2013; accepted 31 December 2013

The production mechanism of single crystalline ZnO nanoscale rods, either in array or block form has been reported alongwith their optical emission characteristics. The elongated vertical nanorods have been characterized by a preferred growth direction along (002) crystallographic plane which becomes prominent with the growth duration. The single-crystalline nature of the nanorods is evident from the electron diffraction studies. Apart from the vertical nanorods, random nanorods and hexagonal shaped nano-blocks have also been found upon changing the pH of the growth solution. With a reference to the relevant growth mechanism of the nanostructures, the optical emission due to band edge and various native defects have been identified via normalized Gaussian fitting incorporated onto the photoluminescence spectra. In contrast to the blocks of nanodisks and random nanorods, the band edge emission (~388 nm) has been found to be significantly enahnced over defect mediated emissions in the vertical nanorods. Owing to long range ordering and enhanced periodicity, single crystalline ZnO would find better scope as compared to conventional polycrystalline systems.

Keywords: Zinc oxide, Single crystal, Nanostructure, Emission

1 Introduction

Zinc oxide (ZnO) is one of the most widely investigated systems owing to promising application in UV-lasing devices[1], gas sensing[2] and cell labeling and tracking[3]. The evolutions of spherically symmetric nanoparticles to asymmetric shaped ZnO structures have gained a great deal of interest in recent years. Accordingly, ZnO nanostructures of a diverse variety, e.g., nanobelts[4], nanorings[5], nanocombs[6], nanodisks[7,8] and nanourchins[9] have been fabricated and tested for suitable applications. Most of these morphologies exhibit hexagonal wurtzite structure and were found in polycrystalline form. Although growth mechanism was different for one morphology to another owing to influence of critical parameters like synthesis temperature, nature of catalyst, reactant concentration, and reaction time, etc., role of active polar crystal surface is generally common to each case. Growing single crystal ZnO in asymmetric morphology is tricky as it involves repetitive addition of unit cells without loss of generality and periodicity. In other words, formation of newer crystals is disallowed between the initiation and termination of growth process of a regular nanostructure. Earlier, attempt was also made to grow single crystalline ZnO nanosystems that exhibited wurtzite phase[10].

*Corresponding author (E-mail: best@tezu.ernet.in)

In the present manuscript, growth mechanism and radiative emission characteristics of stacks of single crystalline ZnO nanorods have been discussed. The structures were derived from the catalyst-free seeded crystals as grown from the solution phase. Synthesis environment dependent morphological aspects, growth mechanism as well as photoluminescence emission characteristics are also highlighted.

2 Experimental Details

The nanorods of ZnO were synthesized grown from a seed layer of ZnO were synthesized using zinc acetate dihydrate (ZAD) [$Zn(CH_3COO)_2.2H_2O$] and sodium hydroxide (NaOH) as reactants. In a typical reduction process, 0.01 M ZAD and 0.03 M NaOH in methanol were prepared separately under a stirring (~250 rpm) environment. The reactants were then subjected to homogeneous mixing at a temperature of 60 °C for about 1 h. The spontaneous decomposition of ZAD and NaOH to form $Zn(OH)_2$ seed crystals was expected due to ion exchange reaction in the solution. A layer of seed crystals was then casted on an ultrasonically cleaned 2 cm×2 cm borosilicate glass substrate and was subjected to heat treatment at ~ 80 °C for about 1 h. Consequently, the decomposition of $Zn(OH)_2$ to ZnO is expected. Upon drying, the slide containing seed layer was immersed in an aqueous solution prepared from 0.05 M zinc nitrate hexahydrate

(ZNH) $[Zn(NO_3)_2.6H_2O]$ and 0.05 M hexamethylenetetramine (HMT) $[(CH_2)_6N_4]$ in deionized water. The solution was further stirred vigorously for varying time duration of 4 and 6 h, while temperature was maintained at 90 °C. The seed crystals of ZnO were expected to facilitate rapid nucleation and consequently, homogeneous growth of nanostructures. Finally, the samples were taken out of the media and rinsed with deionized water several times in order to remove undesired byproducts and un-developed products.

In another occasion, the growth process of the ZnO seeded layer was carried out under varying pH condition. The pH value of the growth solution was controlled at 6 and 10 by considering either addition of dilute HCl or NaOH.

Morphological and structural analyses were performed by scanning electron microscopy (SEM, JSM LV), high resolution transmission electron microscopy (HRTEM, JEOL JSM-2100 CX working under an accelerating voltage of 200 kV) and X-ray diffraction (XRD, Rigaku Miniflex, λ=1.543 Å) studies. The optical absorption and emission properties were explored by using UV-Vis optical absorption spectroscopy (Shimadzu, UV 2450) and steady state photoluminescence emission (PL, PerkinElmer LS55) spectroscopy. All the analytical studies were carried out at room temperature (~300 K).

3 Results and Discussion

Figure 1 depicts the XRD pattern of ZnO nanorods, synthesized with different reaction times. The diffractograms reveal the formation of hexagonal wurtzite phase of ZnO with preferred orientation along (002) crystallographic plane. The higher intensity of the (002) peak over the other peaks, in both the nanorod samples (Fig. 1(a, b)), suggests that the preferential growth has occurred along the *c*-axis or perpendicular to the plane of the substrate. The other diffraction peaks, corresponding to different crystallographic orientation, have aroused owing to the misalignment suffered by a few nanorods[11]. It can be noticed that, in case of the nanorods grown over 6 h duration of reaction time, the intensity of (002) peak has significantly improved as compared to other peaks and a number of peaks adequately suppressed (e.g. (102), (110) are observable for the sample grown over 4 h duration of reaction time). The intensity ratio of the (002) and (101) peak ($I_{(002)}$ /$I_{(101)}$) for the nanorods fabricated with a reaction time of 6 h, is characterized by a higher magnitude (~1.4 times) than the case for nanorods grown in 4 h. It is now apparent that, the preferential growth (along the *c*-axis) of the crystallites would increase for a longer duration of the reaction time which facilitates optimal use of the precursor.

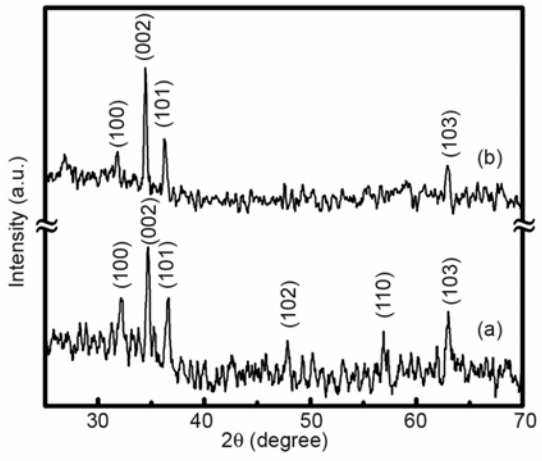

Fig. 1 — XRD patterns of the nanorods grown over a reaction time of (a) 4 h and (b) 6 h

The top view of the uniformly grown ZnO nanorods on the glass substrate can be observed in the SEM micrographs (Fig. 2(a, b)). It can be seen that, most of the nanorods are vertically aligned, while others are top-tilted to different degrees. The visual impression of vertical alignment of the nanorods confirms the XRD result which reveals that the growth process has taken place along a direction perpendicular to the substrate. As evident from the SEM images, the nanorods while maintaining their

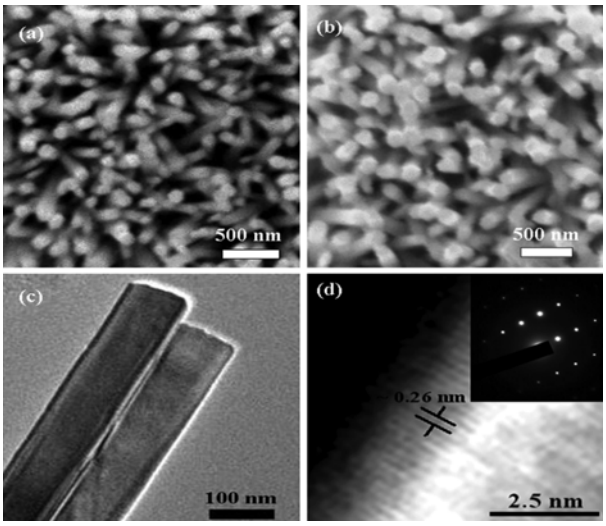

Fig. 2 — SEM images of the nanorods grown over a reaction time of (a) 4 h, (b) 6 h, (c) and (d) HRTEM images of the nanorods. The inset of (d) represents the SAED pattern

independent existence form a highly compact system. The average diameter of the nanorods, synthesized for a reaction time of 4 and 6 h, was found to be ~ 90 and ~ 125 nm; respectively. The reason behind uni-directional and asymmetric growth is expected due to the anisotropic surface energy which depends on the crystal faces of the wurtzite ZnO. Although catalyst mediated growth of elongated ZnO nanostructures has been demonstrated in the past[12,13], the catalyst-free growth mechanism has not yet been explored completely[13,14].

The morphology of fully grown nanorods possessing smooth surface can be seen in the HRTEM image shown in Fig. 2(c). An image has also captured at the edge of a nanorod. In this case, the lattice fringes due to the periodically arrayed crystalline planes of ZnO are clearly observable which shows that inter-planar spacing corresponding to (002) growth plane of the ZnO nanorods is ~ 0.26 nm (Fig. 2(d)). The observation of the periodically arranged (002) plane is also supported by the XRD analysis regarding the growth direction of the nanorods. The selective area electron diffraction (SAED) pattern of the nanorod is shown in the inset of Fig. 2(d). The evolution of distinct, bright spots in the SAED pattern reveals the single crystalline nature of the nanorods. Each spot is the result of constructive scattering from a set of lattice planes of the single crystals. While a minimal percentage of polycrystallinity may be present but it is the singe crystalline nature which dominates the most. Thus it also provides adequate support to the fact of oriented growth of the crystallites along the *c*-axis forming ZnO nanorods.

In contrast to the vertical nanorod arrays, upon varying the pH of the solution, the formation of blocks of hexagonal nanorods and randomly distributed nanorods of ZnO has been witnessed (Fig. 3(a, b)). Figure 3(a) shows the SEM micrograph of the hexagonal-shaped nanoblocks of ZnO obtained at pH 6. Both small and larger units of nanoblocks can be found in the SEM micrograph. The small ones resemble the shape of hexagonal-disks while larger ones, in the form of pillars. In fact, smaller structures are believed to be underdeveloped. A closer view of the nanopillars, with six facets is shown in the inset of the figure. The typical dimension varies in the range of 100-800 nm. In contrast, as shown in Fig. 3(b), fully grown nanorods with typical length scale within 1.5-2 μm and diameter ~100 nm can be obtained upon raising the pH value of the precursor to 10. In this case, the nanorods are found to be randomly distributed over the substrate.

The morphology of the nanostructures is basically originated from two types of growth mechanism; vertical growth and lateral growth. Figure 4 represents a scheme of the nanostructure growth mechanism. The evolution of nanorods and nanoblocks are the consequences of the vertical and lateral growth of the ZnO seed particles. Note that, the ZnO nanoparticles act as the nucleation sites for the growth process. In this process, the Zn^{2+} ions are supplied from the decomposition of ZNH. Whereas, HMT, being a highly water soluble and non-ionic tetradentate cyclic tertiary amine, degrades to give off OH^- ions in the aqueous solution[15]. The chemical reactions associated with this process are given below:

$$(CH_2)_6N_4 + 6H_2O \rightarrow 6HCHO + 4NH_3$$
$$NH_3 + H_2O \rightarrow NH_4^+ + OH^-$$
$$Zn^{2+} + 2OH^- \rightarrow ZnO\ (s) + H_2O$$

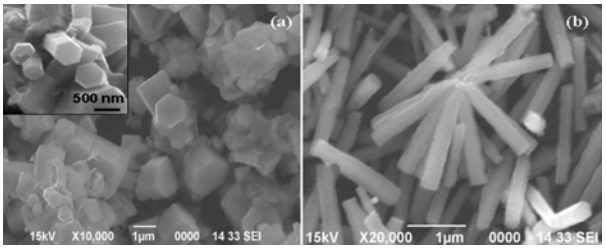

Fig. 3 — SEM images of the nanostructures grown under different pH environment (a) nano-disks (pH=6) and (b) random nanorods (pH=10). Inset of (a) depicts a close look of the nano-disks

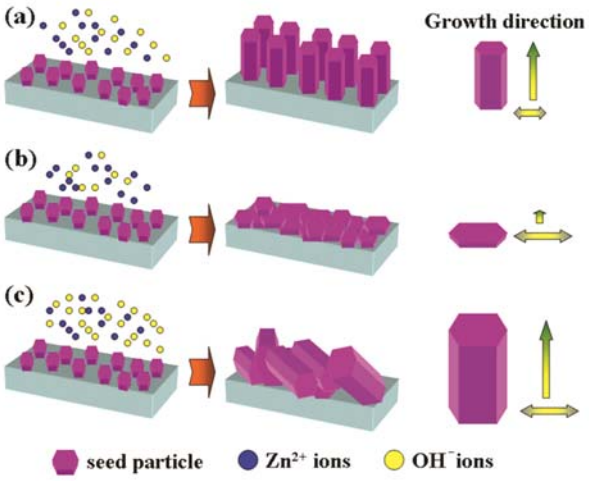

Fig. 4 — Schematic representation of the nanostructure growth mechanism (a) vertical nanorods, (b) blocks of nanodisks and (c) random nanorods

By and large, these seed crystals would act as the nucleating sites for accommodating unit cells maintaining thereby periodicity and structural ordering. The complete structure though initiated from seed crystals is ultimately mediated by the addition of unit cells along a preferential direction. It is worth mentioning here that, growth along a specific direction accounts for the surface energy (γ). As the surface energy of ZnO is drastically different along different directions of the unit cell, the growth would not occur evenly in all directions[9,16]. Consequently, the lateral and vertical growth would compete with each other and the later becomes dominant owing to lower surface energy along the direction of growth[16], i.e., $\gamma_{[0001]} < \gamma_{[1120]} < \gamma_{[1010]}$. In other words, growth along the *c*-direction is energetically favored. Thus each of the nanorods is the outcome of independent but seeded events where lateral growth is substantially hindered. Rapid vertical growth from ZnO seed crystals along [0001] direction could account for the formation of single crystalline elongated nanostructures. Again, the growth process is found to depend on the reaction time. This is evident from the fact that, the diameter of the nanorods grown in 6 h of reaction time, is higher than that of the nanorods grown in 4 h owing to favorable lateral growth.

Now, in the acidic environment (pH value 6) during second step of the synthesis, the concentration of H^+ ions will be more with respect to that of OH^- ions. As a result, successive addition of unit cells, along the preferred direction, and leading to nanostructure growth will be hindered owing to unavailability of OH^- ions. In this circumstance, a number of seed crystals could result in a lateral growth due to the addition of cells in a repetitive manner. Thus the evolution of the hexagonal disk-shaped nanoblocks can be assigned to the dominance of the lateral growth of the seed crystals over the vertical growth (Fig. 3(a)). On the contrary, in the basic medium (pH value 10), the concentration of OH^- ions increases, and the reaction becomes faster along the preferred direction. Comparatively larger diameter of the random nanorods than the vertical ones suggests that, the lateral growth in the former one occurs more rapidly, but it is the vertical growth which dominates in both the growth processes. Owing to the presence of excessive OH^- ions, the initial growth becomes uncontrolled and nonselective and as a result, there could be a random addition of unit cells over the distributed seed crystals. As a result, evolution of randomly distributed nanorods over the substrate is ascertained.

The UV-Visible optical absorption spectra of single crystalline nanoscale structures are shown in Fig. 5(a). As can be found, a strong absorption feature at ~ 355 nm (~3.49 eV) is seen which can be attributed to excitonic absorption corresponding to the lowest available ground state. The higher value of ground state absorption energy, compared to the bulk counterpart (3.3 eV), indicates the formation of low dimensional structures. On the other hand, the random nanorods and nanoblocks exhibit the ground state excitonic absorption within ~ 370 nm (~3.35 eV) regions (Fig. 5(b)). Compared to the vertical nanorods, the red shift in the absorption characteristic of these nanostructures is a consequence of their increased dimension.

The PL emission response (λ_{ex}=300 nm) of vertical nanorod arrays is shown in Fig. 6(a). The emission

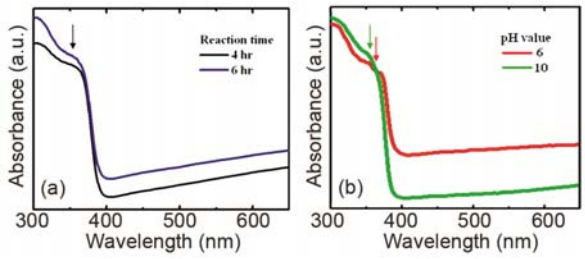

Fig. 5 — Optical absorption spectra of (a) vertical nanorods grown with different reaction time and (b) nanostructures grown with different pH values

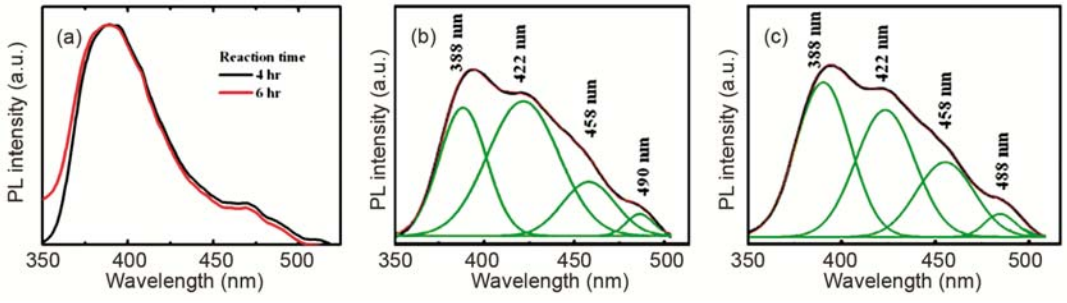

Fig. 6 — Room temperature PL spectra (λ_{ex}=300 nm) of (a) vertical nanorods, (b) blocks of nanodisks and (c) random nanorods

Table 1 — Various emission response as compared to NBE response

Sample	Zn_i	Zn_i^+	V_O^+
Nanodisks	1.1	0.4	0.2
Random nanorods	0.7	0.4	0.1

peak centered at ~ 388 nm corresponds to the typical near band edge emission (NBE) of ZnO. In contrast to the band edge emission, the small emission features, observed at the higher wavelength side, are found to be originated from the various defect related emissions[17] of ZnO. The dominance of the band edge emission and the presence of nominal amount of defect related emission suggest the superior quality of the crystallographic arrangements of the single crystalline nanorods. Now, in absence of single symmetric emission peak that would correspond to a particular radiative process, it is expected that the overall emission feature is due to superimposition of several peaks of different origins. In contrast to the vertical nanorods, the PL spectra of the nanodisks and random nanorods are asymmetrically broadened and stretched. We have employed normalized Gaussian fitting to the experimental curves separately to extract out individual PL-emission peaks. Figure 6(b, c) depicts the deconvoluted PL spectra of the blocks of nanodisks and random nanorods. During the fitting process, the area under the experimental curve is kept as the sum total of the areas under the deconvoluted peaks. The position and width of the fitted peaks have been adjusted so that the empirical curve (red label) formed by the combination of the fitted peaks matches the experimental curve (black label).

The NBE peak is found to be located at ~ 388 nm while other peaks are attributed to defects of different origins. Compared to the vertical nanorod arrays, the presence of more crystal defects in this case has aroused from the unsteady growth process owing to the shortage or abundance of OH^- species due to the pH variation in the solution. The peaks positioned at ~ 422 nm and 458 nm are due to the neutral (Zn_i) and ionized zinc interstitial (Zn_i^+) defects[17-19]. Whereas, the peak identified at ~ 490 nm is ascribed to the singly ionized oxygen vacancy (V_o^+) related defect[20]. A comparative defect mediated emission response of different origins with respect to NBE is presented in Table 1. It may be noted that NBE and Zn_i defect related emission intensities are comparable for the nanodisk specimen (Fig. 6(b)) whereas, the latter is suppressed for the random nanorod system (Fig. 6(c)). The higher concentration of Zn_i defects in the nanodisks might have occurred owing to the insufficient supply of hydroxyl ions in the solution. The higher value of V_o^+ defects in the nanodisks also supports this fact.

While different structures have their own advantage and disadvantages, scope of understanding catalyst-free, single crystalline elongated ZnO is still open to meet various technological challenges where defect emission can be a boon for certain applications.

4 Conclusions

Processing mechanism and steady state emission properties of ZnO nanoscale structures have been demonstrated. Originated from seed crystals, the continuous and uniform growth along *c*-axis of ZnO crystal has been found to result in the formation of single crystalline vertical nanorod arrays. The X-ray diffraction studies suggest the crystallographic growth along [0001] direction of the nanorods, while electron diffraction pattern reveals the single crystalline nature of the nanorods. Again, the acidic medium mediated agglomeration of seed crystals and hindered growth along the *c*-axis are found to be responsible for the evolution of hexagonal shaped nanodisks. On the other hand, the growth of randomly distributed uniform sized nanorods is favored in a basic environment. Moreover, the synthesis dependent nanostructures are also distinguishable in terms of native defect related emission. The superior quality of the single crystalline vertical nanorods is pointed out by the presence of very minute amount of native defect states. Furthermore, the variation of zinc interstitial and oxygen vacancy defects in the nanoblocks and random nanorods can be related to the variation in pH value of the growth solution. Understanding dynamics of native defects in single crystalline nanoscale ZnO will find immense value in polarized light emission devices and nonlinear optics.

Acknowledgements

We are thankful to SAIF, NEHU, Shilong for providing the electron microscopy facility.

References

1 Huang M, Mao S, Feick H, Yan H, Wu Y, Kind H, Weber E, Russo R & Yang P, *Science*, 292 (2001) 1897.
2 Das S N, Kar J P, Choi J H, Lee T I, Moon K J & Myoung J M, *J Phys Chem C*, 114 (2010) 1689.
3 Xiong H, Wang Z, Liu D, Chen J, Wang Y & Xia Y, *Adv Funct Mater*, 15 (2005) 1751.

4 Hughes W L & Wang Z L, *Appl Phys Lett*, 86 (2005) 043106.
5 Kong X Y, Yong D, Yang R & Wang Z L, *Science*, 303 (2004) 1348.
6 Wang Z L, Kong X Y & Zuo J M, *Phys Rev Lett*, 91 (2003) 185502.
7 Gao P X, Lao C S, Yong D & Wang Z L, *Adv Funct Mater*, 16 (2006) 53.
8 Xu C X, Zhu G P, Kasim J, Tan S T, Yang Y, Li X, Shen Z X & Sun X W, *Curr Appl Phys*, 9 (2009) 573.
9 Bayan S & Mohanta D, *J Appl Phys*, 108 (2010) 023512.
10 Wang D, Yang J, Xing G, Yang L, Lang J, Gao M, Yao B & Wu T, *J Lumin*, 129 (2009) 996.
11 Mamat M H, Khusaimi Z, Zahidi M M, Bakar S A, Siran Y M, Rejab S A M, Asis A J, Tahiruddin S, Abdullah S & Mahmood M R, *Jpn J Appl Phys*, 50 (2011) 06GH04.
12 Özgür Ü, Alivov Y I, Liu C, Teke A, Reshchikov M A, Doğan S, Avrutin V, Cho S J & Morkoç H, *J Appl Phys*, 98 (2005) 041301.
13 Yi G C, Wang C & Park W I, *Semicond Sci Technol*, 20 (2005) S22.
14 Park W I, Yi G C, Kim M Y & Pennycook S, *Adv Mater*, 14 (2002) 1841.
15 Baruah S & Dutta J, *Sci Technol Adv Mater*, 10 (2009) 013001.
16 Fujimura N, Nishihara T, Goto S, Xu J & Ito T, *J Cryst Growth*, 130 (1993) 269.
17 Lin B, Fu Z & Jia Y, *Appl Phys Lett*, 79 (2001) 943.
18 Lima S A M, Sigoli F A, Jafelicci M & Davolos M R, *Int J Inorg Mater*, 3 (2001) 749.
19 Zhang L L, Guo C X, Chen J G & Hu J T, *Chin Phys*, 14 (2005) 586.
20 Ye J D, Gu S L, F Qin, Zhu S M, Liu S M, Zhou X, Liu W, Hu L Q, Zhang R, Shi Y & Zheng Y D, *Appl Phys A Mater Sci Process*, 81 (2005) 759.